[13] Crystal data for **15**: $M_r = 1001.44$, monoclinic, space group $P2_1$, $a = 1073.7(1)$, $b = 2317.0(2)$, $c = 1756.3(1)$ Å, $\beta = 97.03(1)^\circ$, $V = 4336.4(6)$ Å^3, $Z = 4$, $\rho_{calcd} = 1.534$ Mg m^{-3}, $Mo_{K\alpha}$ radiation ($\lambda = 0.71073$ Å), $\mu = 0.847$ mm^{-1}. Data were collected on a STOE IPDS system at 193 K. The structure was solved by direct methods and refined on F_0^2 by full-matrix least-squares methods (SHELXS-97, SHELXL-97, SHELDRICK, 1997). All non-hydrogen atoms were refined anisotropically. $\omega R2 = 0.0893$ (all unique data), $R1 = 0.0367$ for data with $I > 2\sigma(I)$. Crystallographic data (excluding structure factors) for the structure reported in this paper have been deposited with the Cambridge Crystallographic Data Centre as supplementary publication no. CCDC-134965. Copies of the data can be obtained free of charge on application to CCDC, 12 Union Road, Cambridge CD21EZ, UK (fax: (+44) 1223-336-033; e-mail: deposit@ccdc.cam.ac.uk).

[14] Selected ^{31}P NMR data (81 MHz, $CDCl_3$) of the phosphane ligands **2** and their complexes with Rh^{I}: **2a**: $\delta = -16.7$ (d, $J_{P,P} = 19.1$ Hz), -23.2 (d, $J_{P,P} = 19.1$ Hz); [Rh(nbd)(**2a**)]BF_4: $\delta = 23.1$ (dd, $J_{P,P} = 22.0$, $J_{P,Rh} = 129.7$ Hz), 8.6 (dd, $J_{P,P} = 22.0$, $J_{P,Rh} = 117.6$ Hz); **2b**: $\delta = -17.1$ (d, $J_{P,P} = 20.3$ Hz), -22.4 (d, $J_{P,P} = 20.3$ Hz); [Rh(nbd)(**2b**)]BF_4: $\delta = 24.4$ (dd, $J_{P,P} = 30.5$, $J_{P,Rh} = 155.1$ Hz), 5.1 (dd, $J_{P,P} = 30.5$, $J_{P,Rh} = 153.2$ Hz); **2c**: $\delta = -12.9$ (d, $J_{P,P} = 18.4$ Hz), -22.4 (d, $J_{P,P} = 18.4$ Hz); [Rh(nbd)(**2c**)]BF_4: $\delta = 17.9$ (dd, $J_{P,P} = 23.5$, $J_{P,Rh} = 101.9$ Hz), 16.0 (dd, $J_{P,P} = 23.5$, $J_{P,Rh} = 101.9$ Hz); **2d**: $\delta = -17.8$ (d, $J_{P,P} = 26.7$ Hz), -22.8 (d, $J_{P,P} = 26.7$ Hz); [Rh(nbd)(**2d**)]BF_4: $\delta = 24.8$ (dd, $J_{P,P} = 31.1$, $J_{P,Rh} = 155.1$ Hz), 12.3 (dd, $J_{P,P} = 31.1$, $J_{P,Rh} = 155.1$ Hz).

Dendritic Iron Porphyrins with Tethered Axial Ligands: New Model Compounds for Cytochromes**

Philipp Weyermann, Jean-Paul Gisselbrecht, Corinne Boudon, François Diederich,* and Maurice Gross

Dedicated to Professor Jean-Marie Lehn on the occasion of his 60th birthday

The most intriguing characteristics of the cytochrome family of electron transfer proteins is the very broad range of redox potentials featured by the Fe^{III}/Fe^{II} couple at the electroactive heme core.[1] A variety of model studies have identified a dependency of this potential from the nature of substituents at the porphyrin ring,[2] axial ligation to the iron center,[3] hydrogen bonding to the axial ligands,[4] and ruffling of the porphyrin macrocycle.[5] In contrast, the influence of environmental effects such as heme solvation,[6] polarity of the heme microenvironment,[7] and the nature of the surrounding protein shell[8] have not been intensively investigated using model compounds and are less well understood.

We have already reported the use of dendritic iron porphyrins[9, 10] as model compounds for cytochromes in which the protein shell around the buried electroactive core is mimicked by the dendritic superstructure. These investigations revealed a strong correlation between the redox potential and the degree of dendritic branching. In these early systems, however, the nature of the axial ligation to the iron center, which is known to have a very strong influence on the redox properties[3] was not controlled. Therefore, the observed shifts in redox potential caused by the dendritic shell could not be quantified independently from axial ligation effects and no general conclusions concerning the effects of the dendritic superstructure could be drawn.

We now present a new series of dendritic cytochrome mimics, which contain a defined and stable axial ligation pattern. This allows, for the first time, a quantitative evaluation of the effect of an insulating dendritic shell on the redox properties of the embedded iron porphyrin core. The three novel dendrimers of generation zero ([**1**·Fe]Cl), one ([**2**·Fe]Cl), and two ([**3**·Fe]Cl) feature controlled axial ligation at the iron center by two imidazoles tethered to the porphyrin core. This stable ligation pattern, which is kinetically inert towards coordinating solvents, is found in the cytochrome b_5 family of electron transfer proteins.[11] The optimal length of the alkyl tethers between the iron-coordi-

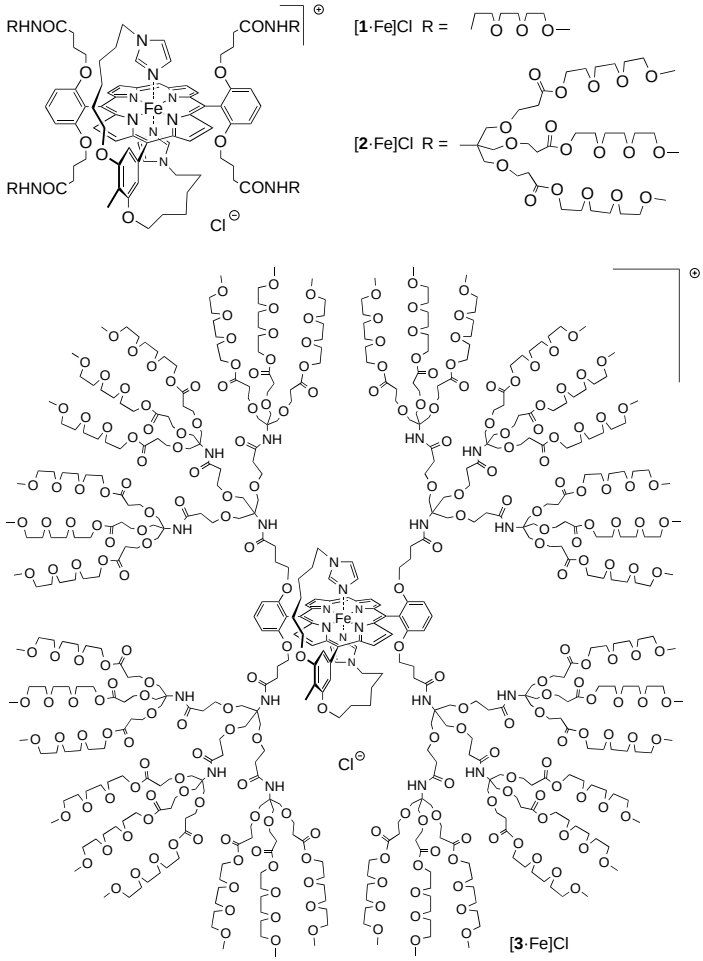

[*] Prof. Dr. F. Diederich, Dipl.-Chem. P. Weyermann
Laboratorium für Organische Chemie, ETH-Zentrum
Universitätstrasse 16, CH-8092 Zürich (Switzerland)
Fax: (+41) 1-632-1109
E-mail: diederich@org.chem.ethz.ch
Dr. J. P. Gisselbrecht, Dr. C. Boudon, Prof. Dr. M. Gross
Laboratoire d'Electrochimie et de Chimie Physique du Corps Solide
Faculte de Chimie, Universite Louis Pasteur and CNRS, UMR no. 7512
4, rue Blaise Pascal, F-67000 Strasbourg (France)

[**] This work was supported by the ETH Research Council.

nating imidazoles and the phenyl ring at the porphyrin core was designed with the help of molecular modeling.[12] The second-generation compound [**3**·Fe]Cl (11719 Da) is comparable in mass to typical single-heme cytochromes such as cytochrome c (tuna, 11384 Da),[13] or cytochrome b_5 (bovine, 15198 Da).[11] With their triethyleneglycol monomethyl ether surface groups, the three dendritic mimics are soluble in solvents of widely differing polarity.

The key intermediate in the synthesis of the dendritic porphyrins was the bis-imidazole-appended zinc porphyrin **4**·Zn, which was obtained in high yield by a Suzuki coupling between the brominated zinc porphyrin **5**·Zn and the bis-imidazole-appended phenylboronic ester **6** (Scheme 1). The *meso*-bromoporphyrin **5**·Zn was obtained from precursor **7**·H_2[9c] by dibromination with *N*-bromosuccinimide (NBS) to

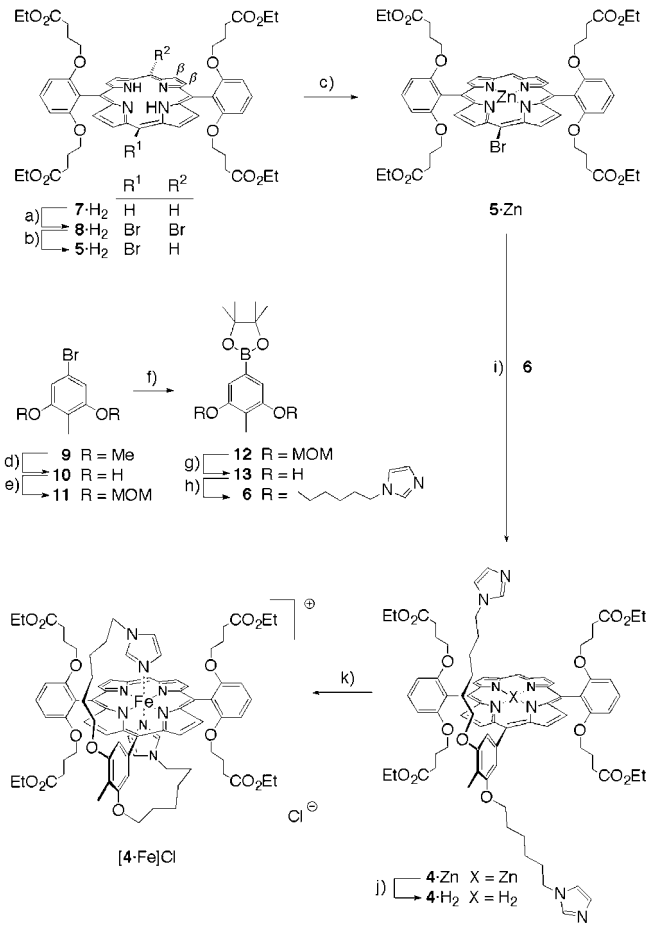

Scheme 1. Synthesis of the bis-imidazole-ligated Fe^{III} porphyrin core [**4**·Fe]Cl. a) NBS (2.0 equiv), $CHCl_3$, RT, 30 min, 91%; b) nBu_3SnH (1.5 equiv), AIBN (0.1 equiv), PhH, reflux, 4 h, 45%; c) $Zn(OAc)_2$ (10.0 equiv), $CHCl_3$/MeOH, RT, 4 h, 98%; d) conc. HI (excess), AcOH, reflux, 6 h, 95%; e) MOM-Cl (4.0 equiv), K_2CO_3 (8.0 equiv), MeCN, 0 °C, 30 min, 98%; f) *n*BuLi (1.6 equiv), TMEDA (1.6 equiv), THF, −78 °C, 60 min, then $B(OMe)_3$ (5.0 equiv), RT, 2 h, then pinacol (10.0 equiv), PhH, reflux, 12 h, 96%; g) conc. HCl (excess), THF/MeOH, RT, 3 d, 66%; h) **14** (5.0 equiv), Cs_2CO_3 (10.0 equiv), DMF, RT, 4 h, 49%; i) **6** (2.0 equiv), $[Pd(PPh_3)_4]$ (0.1 equiv), Cs_2CO_3 (8.0 equiv), PhMe, 90 °C, 4 h, 82%; j) CF_3COOH (excess), $CHCl_3$, 0 °C, 5 min, 78%; k) $FeCl_2$ (10.0 equiv), 2,6-lutidine (10.0 equiv), THF, reflux, 2 h, then 1% HCl in $CHCl_3$ (excess), RT, 5 min, then "proton sponge" (excess), THF, RT, 15 min, 66%. AIBN = $\alpha\alpha'$-azobis(isobutyronitrile); MOM = methoxymethyl; TMEDA = *N,N,N′,N′*-tetramethylethylenediamine; DMF = *N,N*-dimethylformamide; "proton sponge" = 1,8-bis(dimethylamino)naphthalene.

give *meso*-dibromoporphyrin **8**·H_2, partial reduction with nBu_3SnH to give monobromoporphyrin **5**·H_2, and metalation. Phenylboronic ester **6** was prepared from 4-bromo-2,6-dimethoxytoluene **9**[14] by cleavage of the methyl ethers (conc. HI; →**10**) reprotection of the phenolic hydroxy groups with chloromethyl methyl ether (MOM-Cl; →**11**), metalation (*n*BuLi) and boronic ester formation ($B(OMe)_3$, then pinacol; →**12**), cleavage of the MOM protecting groups (HCl; →**13**), and alkylation with 1-(6-bromohexyl)imidazole (**14**).[15] The Fe^{III} complex [**4**·Fe]Cl was obtained from **4**·Zn by acid-induced demetalation (→**4**·H_2) and subsequent insertion of Fe^{II} ($FeCl_2$), followed by air oxidation.

Comparison of the Fe^{III} complex [**4**·Fe]Cl with the six-coordinate Fe^{III} complex [**7**·Fe(*N*-MeIm)$_2$]Cl[16] (*N*-MeIm = 1-methylimidazole) unambiguously showed complete intramolecular axial coordination of the two tethered imidazoles under formation of a paramagnetic low-spin complex. The UV/Vis[17] and EPR spectra[18] as well as the magnetic moments,[19] determined by the Evans–Scheffold method[20] of both compounds compared very well with those of other bis-imidazole-coordinated Fe^{III} porphyrins. Reduction of [**4**·Fe]Cl, similar to that of [**7**·Fe(*N*-MeIm)$_2$]Cl, with $Na_2S_2O_4$ produced a diamagnetic low-spin complex with a hemochrome absorption spectrum which was readily identified as that of a six-coordinate Fe^{II} species.[21]

For the preparation of the dendritic porphyrins of generation zero (**1**·Zn), one (**2**·Zn), and two (**3**·Zn), the core tetraacid **15**·Zn, obtained by hydrolysis of **4**·Zn, was coupled to the corresponding dendritic wedges **16**–**18**,[22] respectively, using HATU as coupling reagent (Scheme 2). They were purified by preparative gel permeation chromatography (GPC, Biorad Biobeads SX-1, CH_2Cl_2) and fully characterized by standard spectroscopic methods (Table 1). In the Zn^{II} porphyrin derivatives, one imidazole is complexed to the metal ion forming a dynamic five-coordinate species. Demetalation to the highly air- and light-sensitive free-base porphyrins and iron insertion finally yielded the target compounds [**1**·Fe]Cl, [**2**·Fe]Cl, and [**3**·Fe]Cl which were purified by GPC (Biorad Biobeads SX-3, CH_2Cl_2) and shown by MALDI-TOF mass spectrometry to be free of any structural defects. According to UV/Vis and EPR spectroscopy, they are six-coordinate low-spin complexes with double axial imidazole ligation (Table 1). Reduction with $Na_2S_2O_4$ in various solvents led instantaneously to typical low-spin Fe^{II} porphyrin absorption spectra, regardless of the size of the dendrimer.

The redox properties of [**1**·Fe]Cl–[**3**·Fe]Cl were first investigated in the rather nonpolar solvent CH_2Cl_2 using cyclic (CV) and steady-state voltammetry (SSV). All three compounds showed a reversible one-electron reduction step (Figure 1) which was clearly assigned to the Fe^{III}/Fe^{II} couple by spectroelectrochemical methods: the UV/Vis spectra of the electrochemically reduced species were identical to those obtained by chemical reduction, and well defined isosbestic points evolved during controlled potential electrolysis. The generation zero complex [**1**·Fe]Cl exhibited a redox potential of −0.21 V (vs. SCE; Table 2). This is in the expected range for a bis-imidazole-ligated iron porphyrin complex.[23] In the higher generation compounds [**2**·Fe]Cl (+0.08 V) and

  1433-7851/99/3821-3216 $ 17.50+.50/0 *Angew. Chem. Int. Ed.* **1999**, *38*, No. 21

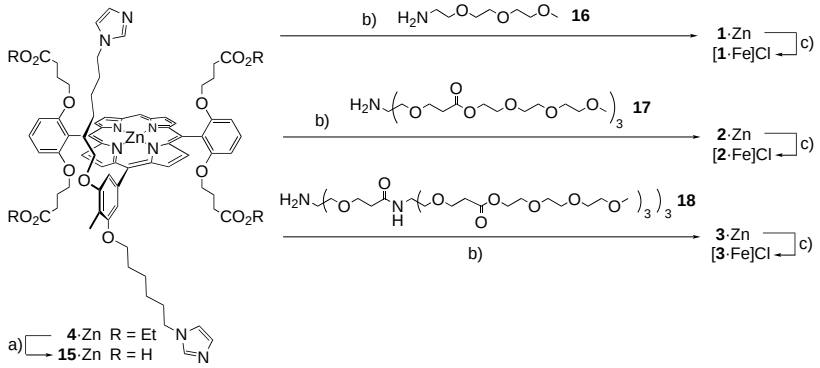

Scheme 2. Synthesis of the dendritic cytochrome mimics [**1**·Fe]Cl–[**3**·Fe]Cl. a) NaOH (excess), dioxane/H_2O, RT, 3 d; b) **16**, **17**, or **18** (12.0 equiv), HATU (6.0 equiv), Et_3N (24.0 equiv), DMF, 0 °C, 24 h, 85 % (**1**·Zn); 3 d, 65 % (**2**·Zn); 7 d, 42 % (**3**·Zn); all yields starting from **4**·Zn; c) TFA (excess), $CHCl_3$, 0 °C, 5 min, then $FeCl_2$ (10.0 equiv), 2,6-lutidine (10.0 equiv), THF, reflux, 4 h, then 1 % HCl in $CHCl_3$ (excess), RT, 5 min, then "proton sponge" (excess), THF, RT, 15 min, 68 % ([**1**·Fe]Cl); 73 % ([**2**·Fe]Cl); 78 % ([**3**·Fe]Cl). HATU = *O*-(7-azabenzotriazol-1-yl)-*N,N,N′,N′*-tetramethyluronium hexafluorophosphate.

Table 1. Selected physical and spectroscopic data of **3**·Zn and [**3**·Fe]Cl.[a]

3·Zn: Viscous purple oil. $R_f = 0.48$ (SiO_2, CH_2Cl_2/MeOH 90:10); UV/Vis ($CHCl_3$): $\lambda_{max}(\varepsilon) = 595$ (5100), 559 (20700), 520 (4200), 427 (544900), 408 (sh, 63600), 311 nm (22500); IR ($CHCl_3$): $\tilde{\nu} = 2880$m, 1735s, 1670m, 1580w, 1520m, 1460m, 1380w, 1355w, 1325w, 1245m, 1185s, 1110s, 1030w, 990w, 950w, 855m, 810w, 620w cm^{-1}; ^1H NMR (500 MHz, [D_5]pyridine, 300 K): $\delta = 10.20$ (s, 1H), 9.47 (d, $J = 4.0$ Hz, 2H), 9.28–9.32 (m, 4H), 9.23 (d, $J = 4.0$ Hz, 2H), 8.05 (br. s, 2H), 8.02 (t, $J = 7.9$ Hz, 2H), 7.52 (s, 2H), 7.49 (d, $J = 7.9$ Hz, 4H), 7.40 (br, s, 2H), 7.31 (br, s, 2H), 6.30 (br, s, 16H), 4.48–4.52 (m, 4H), 4.41–4.45 (m, 4H), 4.32–4.40 (m, 72H), 4.10–4.22 (m, 8H), 3.47–4.05 (m, 576H), 3.29 (s, 108H), 2.69 (t, $J = 6.2$ Hz, 72H), 2.67 (s, 3H), 1.55–1.73 (m, 24H), 1.42–1.54 (m, 4H), 1.21–1.32 (m, 4H); ^{13}C NMR (125 MHz, [D_5]pyridine, 300 K): $\delta = 172.4$, 171.7, 171.4, 160.6, 155.9, 151.3, 151.2, 150.3, 150.2, 142.8, 136.7, 132.0, 132.0, 131.9, 131.4, 130.7, 128.3, 122.1, 120.6, 120.3, 113.2, 113.1, 113.0, 106.2, 105.3, 72.3, 70.8, 70.8, 70.7, 69.7, 69.7, 69.3, 68.7, 68.4, 68.2, 67.3, 64.0, 60.6, 60.6, 58.7, 47.4, 37.3, 35.2, 32.1, 31.1, 29.4, 26.4, 25.9, 24.9, 9.2; MALDI-TOF-MS (2-(4′-hydroxyphenylazo)benzoic acid): *m/z* (%): 11750.8 (100, $[M + Na]^+$, calcd for $C_{533}H_{918}N_{24}O_{250}Zn \cdot Na^+$: 11750.9),[b] 11729.5 (37, M^+, calcd for $C_{533}H_{918}N_{24}O_{250}Zn^+$: 11727.9).[b]

[**3**·Fe]Cl: Viscous brown oil. $R_f = 0.32$ (SiO_2, CH_2Cl_2/MeOH 90:10); UV/Vis ($CHCl_3$): $\lambda_{max}(\varepsilon) = 543$ (10200), 415 (128000), 313 nm (25400); IR ($CHCl_3$): $\tilde{\nu} = 2915$s, 2880s, 1735s, 1670m, 1580w, 1515m, 1460m, 1380w, 1350w, 1320w, 1240m, 1185s, 1110s, 1030w, 995w, 950w, 850w, 620w cm^{-1}; EPR (X-Band, $CHCl_3$, 77 K): $g_x = 1.558$, $g_y = 2.321$, $g_z = 2.890$; MALDI-TOF-MS (2-(4′-hydroxyphenylazo)benzoic acid): *m/z* (%): 11719.2 (100, $[M - Cl]^+$, calcd for $C_{533}H_{918}N_{24}O_{250}Fe^+$: 11718.9).[b]

[a] All new compounds were fully characterized by ^1H and ^{13}C NMR (except Fe complexes), IR, UV/Vis and FAB or MALDI-TOF mass spectra as well as by elemental analysis or high-resolution mass spectra. For all Fe complexes, EPR spectra were recorded and in some cases magnetic moments were calculated by the method of Evans and Scheffold. [b] Calculated highest peak in the isotope pattern.

[**3**·Fe]Cl (+0.10 V), the $Fe^{III} \rightarrow Fe^{II}$ reduction becomes greatly facilitated, with the largest change in potential occurring between generation zero and one.

CV measurements in MeCN, a solvent of intermediate polarity, showed a similar trend: upon changing from generation zero (−0.24 V) to two (+0.09 V), reduction of Fe^{III} becomes increasingly favored (by 330 mV) with the largest change in potential again occurring at the stage of the generation one dendrimer (−0.01 V).

In H_2O, the redox process could only be monitored electrochemically for the generation zero complex, with the generation one dendrimer showing a very weak spread-out reduction step and the second-generation compound being electrochemically silent.[10a] Therefore, we changed to chemical methods to determine the redox potential for the Fe^{III}/Fe^{II} couple in this solvent. UV/Vis spectroscopic investigations showed that equilibria with solutions of suitable reducing agents were rapidly established after mixing with the porphyrin dendrimers. This allowed an accurate, highly reproducible determination of the redox potentials from equilibrium measurements using $[Fe(ox)_3]^{-4}/[Fe(ox)_3]^{-}$[24a, b] or $[Fe(CN)_6]^{-4}/[Fe(CN)_6]^{-3}$[24c, d] (Figure 2), as it is commonly done with proteins.[25] The potentials measured for [**1**·Fe]Cl by chemical and electrochemical methods were in excellent agreement. In contrast to the results obtained in the organic solvents, the potential of the Fe^{III}/Fe^{II} couple hardly shifts upon

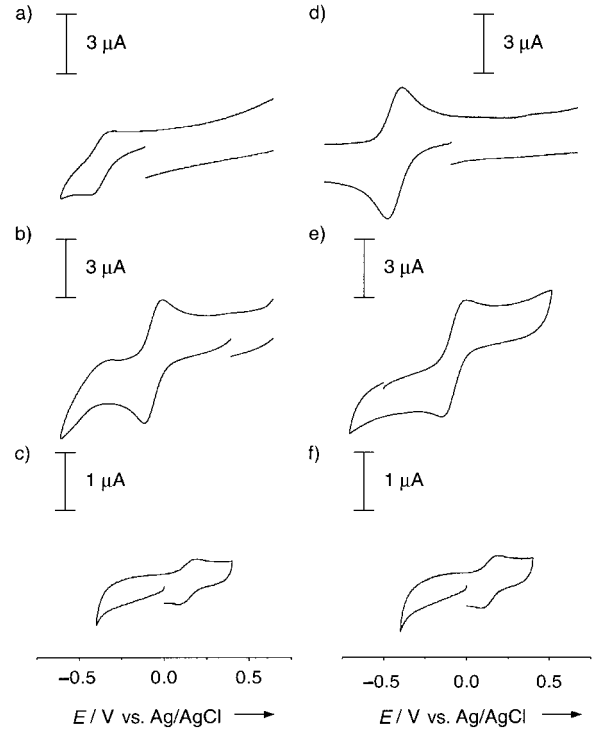

Figure 1. Cyclic voltammograms showing the first reduction step of [**1**·Fe]Cl (a, d), [**2**·Fe]Cl (b, e), and [**3**·Fe]Cl (c, f) in CH_2Cl_2 (left) and MeCN (right). For the conditions, see Table 2.

changing from generation zero (−0.29 V) to one (−0.25 V) but a dramatic increase is observed upon changing to the generation two dendrimer [**3**·Fe]Cl (+0.09 V) (see Table 2). For comparison, the Fe^{III}/Fe^{II} redox potential of cytochrome b_5 in H_2O was determined as +0.24 V vs. SCE.[11b]

The results of the redox studies in the three solvents are summarized in Figure 3: 1) In all solvents, the redox potential of the Fe^{III}/Fe^{II} couple becomes more positive with increasing dendritic generation. Remarkably, the potential of the

Table 2. Redox potentials (in V vs. SCE) of the Fe^{III}/Fe^{II} couple of [**1**·Fe]Cl – [**3**·Fe]Cl in different solvents.

Porphyrin	$E(Fe^{III}/Fe^{II})$		
	CH_2Cl_2[a]	MeCN[a]	H_2O
[**1**·Fe]Cl	−0.21	−0.24	−0.29[b]
[**2**·Fe]Cl	+0.08	−0.01	−0.25[b]
[**3**·Fe]Cl	+0.10	+0.09	+0.09[c]

[a] Values from CV approximated as $E_{1/2} = (E_{pa} - E_{pc})/2$; supporting electrolyte 0.1 M Bu_4NPF_6; glassy carbon working electrode, Ag/AgCl reference electrode, platinum wire counter electrode; $T = 298$ K; scan rate = 0.1 V s^{-1}; typical concentration 5×10^{-4} M; ferrocene was used as an internal standard, and the redox potentials referenced against the standard calomel electrode (SCE) using published values for the Fc/Fc^+ couple in CH_2Cl_2 (0.46 V vs. SCE; N. G. Connelly, W. E. Geiger, *Chem. Rev.* **1996**, *96*, 877 – 910) and MeCN (0.45 V vs. SCE; W. G. Barrette, Jr., H W. Johnson, Jr., D. T. Sawyer, *Anal. Chem.* **1984**, *56*, 1890 – 1898). [b] Values from equilibrium measurements with $[Fe(ox)_3]^{-4}/[Fe(ox)_3]^{-3}$ (ox = oxalate) as reference compound.[26] [c] Values from equilibrium measurements with $[Fe(CN)_6]^{-4}/[Fe(CN)_6]^{-3}$ as reference compound.[26]

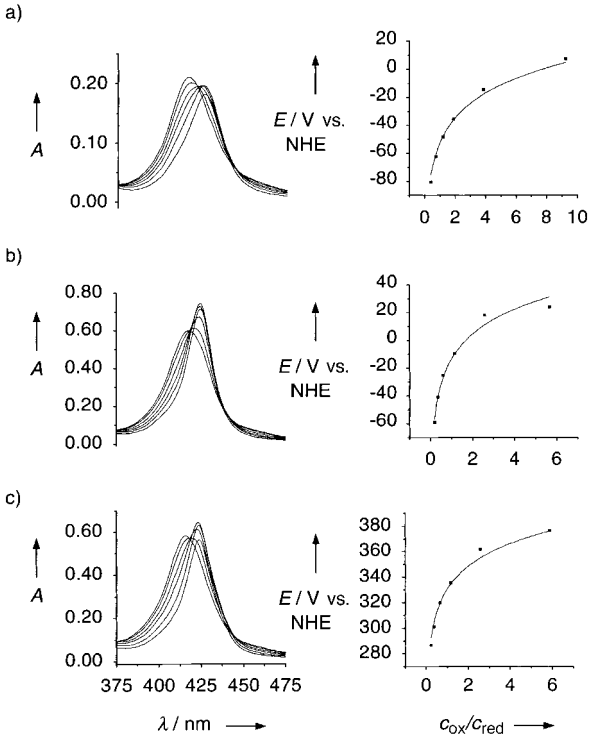

Figure 2. Redox equilibria in H_2O between $[Fe(ox)_3]^{-4}/[Fe(ox)_3]^{-3}$ and [**1**·Fe]Cl (a) and [**2**·Fe]Cl (b) and between $[Fe(CN)_6]^{-4}/[Fe(CN)_6]^{-3}$ and [**3**·Fe]Cl (c). Spectral evolution of the Soret band region in the UV/Vis spectrum during reductive titration (left) and nonlinear least-squares fit of the titration data to the Nernst equation, yielding the redox potential (right). For the conditions, see Table 2. c_{ox}/c_{red} is the concentration ratio of oxidized and reduced porphyrin.

second-generation complex [**3**·Fe]Cl is, within experimental error, identical in all three solvents (of extremely different polarity), which clearly demonstrates that the dendritic branching creates a unique local microenvironment around the isolated electroactive core. Therefore, the dendritic shell fully mimics the protecting peptide shell which modulates the redox potential of the Fe^{III}/Fe^{II} couple in a similar way in cytochromes.[7a,b] 2) In the two organic solvents, the largest

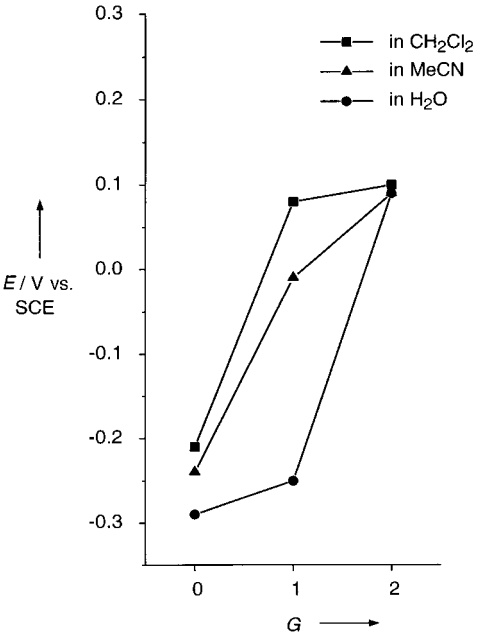

Figure 3. Plot of the redox potentials (in V vs. SCE) of the Fe^{III}/Fe^{II} couple in [**1**·Fe]Cl – [**3**·Fe]Cl in CH_2Cl_2, MeCN and H_2O vs. dendrimer generation *G*.

shift to more positive potential occurs upon changing from the generation zero to the generation one complex. Clearly, the special microenvironment is already largely created by the first generation branching in these solvents. 3) In sharp contrast, the redox potential in H_2O does not vary much upon passing from the generation zero to the generation one complex. Solvation effects are much more pronounced in H_2O, and, as we had previously suggested,[9b,c] the relatively open dendritic branches in [**2**·Fe]Cl do not impede access of bulk solvent to the central core for stabilization of the Fe^{III} state. However in [**3**·Fe]Cl, the dendritic superstructure is sufficiently dense to prevent the contact between the porphyrin and the external bulk solvent, thereby creating the same, unique core microenvironment as in the organic solvents.

This model study confirms the large contributions of the densely packed protein shell to the strong positive shifts of the Fe^{III}/Fe^{II} potential in cytochromes[7a,b] and firmly establishes well-designed dendrimers as powerful mimics for globular proteins.

Received: June 1, 1999 [Z13494IE]
German version: *Angew. Chem.* **1999**, *111*, 3400 – 3404

Keywords: dendrimers · electrochemistry · porphyrinoids · redox chemistry · voltammetry

[1] a) G. R. Moore, G. W. Pettigrew, *Cytochromes-c: Evolutionary, Structural and Physicochemical Aspects*, Springer, Berlin, **1990**; b) F. S. Mathews, *Prog. Biophys. Mol. Biol.* **1985**, *45*, 1 – 56.

[2] a) K. M. Kadish, M. M. Morrison, L. A. Constant, L. Dickens, D. G. Davis, *J. Am. Chem. Soc.* **1976**, *98*, 8387 – 8390; b) A. Giraudeau, H. J. Callot, J. Jordan, I. Ezhar, M. Gross, *J. Am. Chem. Soc.* **1979**, *101*, 3857 – 3862.

  1433-7851/99/3821-3218 $ 17.50+.50/0

[3] a) H. A. Harbury, J. R. Cronin, M. W. Fanger, T. P. Hettinger, A. J. Murphy, Y. P. Myer, S. N. Vinogradov, *Proc. Natl. Acad. Sci. USA* **1965**, *54*, 1658 – 1664; b) P. K. Warme, L. P. Hager, *Biochemistry* **1970**, *9*, 1606 – 1614; c) J. C. Marchon, T. Mashiko, C. A. Reed, *Electron Transport and Oxygen Utilization* (Ed.: C. Ho), Elsevier, North Holland, **1982**, 67 – 72; d) S. G. Sligar, K. D. Egeberg, J. T. Sage, D. Morikis, P. M. Champion, *J. Am. Chem. Soc.* **1987**, *109*, 7896 – 7897; e) A. L. Raphael, H. B. Gray, *J. Am. Chem. Soc.* **1991**, *113*, 1038 – 1040.

[4] a) R. Quinn, J. Mercer-Smith, J. N. Burstyn, J. S. Valentine, *J. Am. Chem. Soc.* **1984**, *106*, 4136 – 4144; b) P. O'Brien, D. A. Sweigart, *Inorg. Chem.* **1985**, *24*, 1405 – 1409.

[5] a) K. M. Barkigia, L. Chantranupong, K. M. Smith, J. Fajer, *J. Am. Chem. Soc.* **1988**, *110*, 7566 – 7567; b) K. M. Kadish, E. van Caemelbecke, P. Boulas, F. D'Souza, E. Vogel, M. Kisters, C. J. Medforth, K. M. Smith, *Inorg. Chem.* **1993**, *32*, 4177 – 4178.

[6] a) E. Stellwagen, *Nature* **1978**, *275*, 73 – 74; b) K. M. Kadish, L. A. Bottomley, S. Kelly, D. Schaeper, L. R. Shiue, *Biolelectrochem. Bioenerg.* **1981**, *8*, 213 – 222; c) L. A. Bottomley, K. M. Kadish, *Inorg. Chem.* **1981**, *20*, 1348 – 1357.

[7] a) R. J. Kassner, *Proc. Natl. Acad. Sci. USA* **1972**, *69*, 2263 – 2267; b) R. J. Kassner, *J. Am. Chem. Soc.* **1973**, *95*, 2674 – 2677; c) A. K. Churg, A. Warshel, *Biochemistry* **1986**, *25*, 1675 – 1681; d) D. Lexa, M. Momenteau, P. Rentien, G. Rytz, J. M. Savéant, F. Xu, *J. Am. Chem. Soc.* **1984**, *106*, 4755 – 4765; e) C. Gueutin, D. Lexa, M. Momenteau, J. M. Savéant, F. Xu, *Inorg. Chem.* **1986**, *25*, 4294 – 4307.

[8] a) M. S. Caffrey, M. A. Cusanovich, *Arch. Biochem. Biophys.* **1991**, *285*, 227 – 230; b) K. K. Rodgers, S. G. Sligar, *J. Am. Chem. Soc.* **1991**, *113*, 9419 – 9421.

[9] a) P. J. Dandliker, F. Diederich, M. Gross, C. B. Knobler, A. Louati, E. M. Sanford, *Angew. Chem.* **1994**, *106*, 1821 – 1824; *Angew. Chem. Int. Ed. Engl.* **1994**, *33*, 1739 – 1742; b) P. J. Dandliker, F. Diederich, J. P. Gisselbrecht, A. Louati, M. Gross, *Angew. Chem.* **1995**, *107*, 2906 – 2909; *Angew. Chem. Int. Ed. Engl.* **1995**, *34*, 2725 – 2728; c) P. J. Dandliker, F. Diederich, A. Zingg, J. P. Gisselbrecht, M. Gross, A. Louati, E. Sanford, *Helv. Chim. Acta* **1997**, *80*, 1773 – 1801.

[10] For other dendritic porphyrins, see: a) K. W. Pollak, J. W. Leon, J. M. J. Fréchet, M. Maskus, H. D. Abruña, *Chem. Mater.* **1998**, *10*, 30 – 38; b) D. L. Jiang, T. Aida, *J. Am. Chem. Soc.* **1998**, *120*, 10895 – 10901; c) P. Bhyrappa, G. Vaijayanthimala, K. S. Suslick, *J. Am. Chem. Soc.* **1999**, *121*, 262 – 263; d) S. A. Vinogradov, L. W. Lo, D. F. Wilson, *Chem. Eur. J.* **1999**, *5*, 1338 – 1347; e) U. Puapaiboon, R. T. Taylor, *Rapid Commun. Mass Spectrom.* **1999**, *13*, 508 – 515.

[11] a) F. S. Mathews, M. Levine, P. Argos, *Nature* **1971**, *233*, 15 – 16; b) S. F. Velick, P. Strittmatter, *J. Biol. Chem.* **1955**, *221*, 265 – 275.

[12] Molecular modeling was performed on a simple Fe^{II} tris(*meso*-phenyl)porphyrin, using the UFF force field implemented in Cerius^2, Version 3.0, BIOSYM Technologies, Inc., San Diego, CA, **1997**.

[13] R. Swanson, B. L. Trus, N. Mandel, G. Mandel, O. B. Kallai, R. E. Dickerson, *J. Biol. Chem.* **1977**, *252*, 759 – 775.

[14] F. P. Doyle, J. H. C. Nayler, H. R. J. Waddington, J. C. Hanson, G. R. Thomas, *J. Chem. Soc.* **1963**, 497 – 506.

[15] F. Montanari, M. Penso, S. Quici, P. Viganò, *J. Org. Chem.* **1985**, *50*, 4888 – 4893.

[16] Directly prepared by dissolving [**7** · Fe]Cl (obtained from **7** · H_2 by iron insertion with $FeCl_2$) in the appropriate solvent, containing 0.1 M *N*-MeIm.

[17] a) H. Kobayashi, T. Higuchi, Y. Kaizu, H. Osada, M. Aoki, *Bull. Chem. Soc. Jpn.* **1975**, *48*, 3137 – 3141; b) F. A. Walker, M. W. Lo, M. T. Ree, *J. Am. Chem. Soc.* **1976**, *98*, 5552 – 5560.

[18] a) J. Peisach, W. E. Blumberg, A. Adler, *Ann. N.Y. Acad. Sci.* **1973**, *206*, 310 – 327; b) G. N. La Mar, F. A. Walker, *J. Am. Chem. Soc.* **1973**, *95*, 1782 – 1790; c) R. Quinn, M. Nappa, J. S. Valentine, *J. Am. Chem. Soc.* **1982**, *104*, 2588 – 2595.

[19] a) L. M. Epstein, D. K. Straub, C. Maricondi, *Inorg. Chem.* **1967**, *6*, 1720 – 1724; b) K. M. Adams, P. G. Rasmussen, W. R. Scheidt, K. Hatano, *Inorg. Chem.* **1979**, *18*, 1892 – 1899.

[20] a) D. F. Evans, *J. Chem. Soc.* **1959**, 2003 – 2005; b) J. Löliger, R. Scheffold, *J. Chem. Educ.* **1972**, *49*, 646 – 647.

[21] a) H. Kobayashi, M. Shimizu, I. Fujita, *Bull. Chem. Soc. Jpn.* **1970**, *43*, 2335 – 2341; b) H. Kobayashi, Y. Yanagawa, *Bull. Chem. Soc. Jpn.* **1972**, *45*, 450 – 456.

[22] T. Habicher, F. Diederich, V. Gramlich, *Helv. Chim. Acta*, **1999**, *82*, 1066 – 1095.

[23] a) L. A. Constant, D. G. Davis, *Anal. Chem.* **1975**, *47*, 2253 – 2260; b) K. M. Kadish, L. A. Bottomley, *Inorg. Chem.* **1980**, *19*, 832 – 836; c) M. J. M. Nesset, N. V. Shokhirev, P. D. Enemark, S. E. Jacobsen, F. A. Walker, *Inorg. Chem.* **1996**, *35*, 5188 – 5200.

[24] a) J. J. Lingane, *J. Am. Chem. Soc.* **1946**, *68*, 2448 – 2453; b) W. B. Schaap, H. A. Laitinen, J. C. Bailar Jr., *J. Am. Chem. Soc.* **1954**, *76*, 5868 – 5872; c) R. C. Murray Jr., P. A. Rock, *Electrochim. Acta* **1968**, *13*, 969 – 975; d) G. I. H. Hanania, D. H. Irvine, W. A. Eaton, P. George, *J. Phys. Chem.* **1967**, *71*, 2022 – 2030.

[25] L. P. Dutton, *Methods Enzymol.* **1978**, *54*, 411 – 435.

[26] A stock solution of fully oxidized porphyrin (typical concentration 5×10^{-6} M) was titrated with a stock solution of fully reduced reference compound (typical concentration 2.5×10^{-4} M), and the concentrations of all species in solution calculated from the spectrophotometrically determined ratio of oxidized to reduced porphyrin and known total concentrations; $T = 298$ K; E values versus the normal hydrogen electrode (NHE) were obtained from a nonlinear least-squares fit of the series of equilibria produced by the titration to the Nernst equation and referenced for comparison against SCE (0.24 V vs. NHE; D. T. Sawyer, A. Sobkowiak, J. L. Roberts, *Electrochemistry for Chemists*, *2nd ed.*, Wiley, New York, **1995**, Chap. 5, pp. 170 – 248). Titrations were reproduced with excellent agreement in triplicate runs.

Novel U-Shaped Systems Containing an Imide-Functionalized Cleft for the Study of Solvent-Mediated Electron Transfer and Energy Transfer: Synthesis and Binding Studies**

Nicholas J. Head, Anna M. Oliver, Kai Look, Nigel R. Lokan, Garth A. Jones, and Michael N. Paddon-Row*

One of the most intensively investigated issues of long-range electron transfer (ET) and energy transfer (EnT) is how the electronic coupling for these processes depends on the nature of the intervening medium between a pair of chromophores.[1] Using structurally well-defined systems, considerable progress has been made in delineating the characteristics of electronic coupling involving saturated hydrocarbon bridges,[1a–c] protein-like pathways,[1d] and the π stacks of base pairs in DNA molecules.[1e]

By contrast, solvent-mediated electronic coupling remains a vexing issue, owing to the dynamic, jostling nature of the solvent molecules which blur the electronic coupling pathways. Progress has recently been made by using novel rigid U-shaped multichromophoric systems, represented by Class I in Figure 1,[2] in which the terminal chromophores face each other across a "rigid" cavity within which a certain number of solvent molecules are present (in a dynamic sense). However, because these systems still do not address the problem of

[*] Prof. M. N. Paddon-Row, Dr. N. J. Head, Dr. A. M. Oliver, Dr. K. Look, N. R. Lokan, G. A. Jones
School of Chemistry
University of New South Wales
Sydney, N.S.W., 2052 (Australia)
Fax: (+61) 2-9385-6141
E-mail: m.paddonrow@unsw.edu.au

[**] We thank the Australian Research Council for support and for the award of a Senior Research Fellowship (to MNP-R).